Chapter 5

Reaction Network of Pyridine Hydrodenitrogenation over Carbide and Sulfide Catalysts

5.1. Introduction

In the previous chapter, the mechanism of carbon-nitrogen bond cleavage for a series of aliphatic amines was investigated over two carbide catalysts and a reference sulfide catalyst. The results suggested that a β-elimination mechanism is the main reaction path for the C-N bond cleavage over all these catalysts. The objective of the present chapter is to examine in detail the reaction network leading to the formation of one of the aliphatic amines, *n*-pentylamine, by hydrogenation of pyridine and hydrogenolysis of piperidine. Our approach is to study the principal reaction steps individually and to learn about their impact on HDN.

It is well known that hydrogenation of the N-heterocyclic ring is required prior to the C-N bond cleavage in HDN reactions [1]. A difficulty arises from the fact that no single limiting step has been identified [1,2,3,4,5,6]. That occurs because the reaction rates for both steps are of a similar order of magnitude and are dependent on the structure of the N-containing compound and the reaction conditions. There is general agreement, however, that the two catalytic functions necessary for HDN, hydrogenation and C-N bond cleavage, are carried out at different catalytic sites [6,7,8,9]. Under industrial conditions, H_2S will always be present as sulfur compounds always accompany nitrogen

compounds in petroleum feedstocks. The presence of H_2S has been studied by several groups and is reported to have a dual effect on the HDN catalytic activity: reduction of hydrogenation rates and promotion of C-N bond cleavage reactions [7].

We choose pyridine HDN because only a few intermediates are formed and because many of the nitrogen compounds, present in petroleum are pyridine derivatives. The reaction scheme can be depicted for this case as a sequential series (Scheme 5.1).

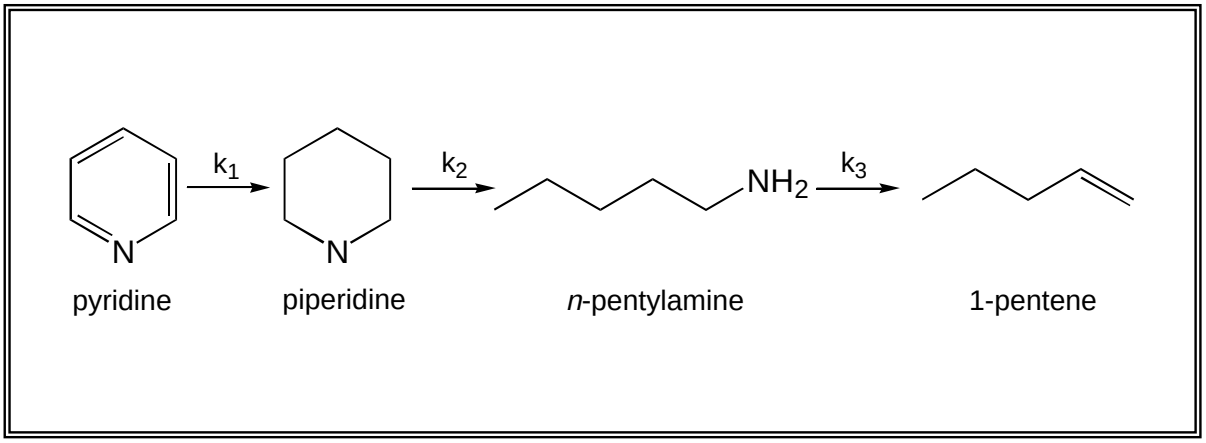

Scheme 5.1. Reaction scheme for HDN of pyridine.

Most of the studies reported deal with the kinetics of pyridine HDN on both sulfided and reduced Ni-Mo and Co-Mo supported on Al_2O_3 [10,11,12,13]. It was found that under most reaction conditions, the first step, hydrogenation of pyridine to piperidine, as well as the second step, formation of pentylamine from C-N bond cleavage of piperidine, are both similarly slow. In order to extend the work to carbide catalysts, knowledge of the conversion rates of pyridine and piperidine relative to *n*-pentylamine is necessary. In summary, the aim of this chapter is to investigate the pyridine HDN and

the role of the intermediates, piperidine and *n*-pentylamine, over Mo_2C, NbC, and $NbMo_2C$, and to compare the results to MoS_2 supported on neutral SiO_2. The reactions are carried out in liquid-phase and high pressures to mimic the characteristic behavior of basic nitrogen compounds under industrial conditions. As will be reported, the behavior of the carbide and sulfide catalysts is remarkably similar, indicating that a common reaction sequence is operative during HDN on these materials. This substantiates the results presented in the previous chapter, which showed that the mechanism of N-removal from amines, β-elimination, was the same on carbides and sulfides.

5.2. Experimental

5.2.1. Materials

Materials used for the preparation of the catalysts were: molybdenum (VI) oxide (MoO_3, 99.95%, Johnson Matthey), niobium (V) oxide (Nb_2O_5, 99.9%, Johnson Matthey), silica (SiO_2, Degussa) with surface area of 90 m^2g^{-1}, and $(NH_4)_6Mo_7O_{24}\cdot 4H_2O$ (Aldrich Chemical Co., A.C.S. reagent). The gases employed were He (Air Products, 99.999 %), CH_4 (Air Products, UHP Grade), H_2 (Air Products, 99.999%), N_2 (Air Products, 99.999 %), 0.5% (v/v) O_2 / He (Air Products, 99.999%), 30 % N_2 / He (Air Products, 99.999%), CO (Air Products, 99.3 %), 10% (v/v) H_2S/H_2 (Air Products, 99.999%). For the reactivity tests, the chemicals employed were: dibenzothiophene (Aldrich, 99.5 %), quinoline (Aldrich, 99.9 %), benzofuran (Aldrich, 99.9 %), tetralin (Aldrich, 99.5 %) and tetradecane (Jansen Chimica, 99 %), pyridine (Aldrich,99 %), piperidine (Aldrich,99 %), *n*-pentylamine (Acros,99 %), dimethyl disulfide (Aldrich, 99

%), octane (Acros, 99 %). All chemicals were used as received. CH_4, H_2, N_2 and 30% N_2/He were passed through water purifiers (Alltech, model # 8121) positioned in the line between the gas cylinders and the reactor, while He and CO were passed through a water/oxygen-removing purifier (Alltech, model # 8121 and 4004).

5.2.2. Synthesis and Characterization of Catalysts

The synthesis and characterization of all the catalysts used are described in detail in the previous chapter. Briefly, the synthesis of the bimetallic carbide involved the solid-state fusion of two monometallic oxides with a metal ratio (Mo/Nb) equal to 2.0 followed by temperature-programmed reaction using a reactive gas flow of 20% CH_4/H_2 up to a temperature of 1063 K. For the preparation of the monometallic Mo_2C and NbC, only the second step applied, with the corresponding single metal oxides being used for the carburization. Two 5.5 wt % MoS_2/SiO_2 catalysts were used as the sulfide references. They were prepared *in situ* by flowing 100 μmol s^{-1} (150 cm^3 min^{-1}, NTP) of 10% H_2S/H_2 over 5 wt% MoO_3/SiO_2 for 2 h at 673 K.

The catalysts were characterized by CO chemisorption (O_2 chemisorption for the sulfide catalysts), temperature programmed desorption (TPD) of ethylamine, N_2 physisorption, and x-ray diffraction (XRD). The values of CO and O_2 chemisorption were used for the calculation of turnover rates. TPD of ethylamine provided a means to count the number of Brønsted acid sites and served as another basis of comparison of catalytic activities. Surface areas were determined by N_2 physisorption, while XRD patterns were acquired using the powder method. The reactivity of all catalysts was tested for HDN of quinoline and HDS of dibenzothiophene in a three-phase, trickle-bed reactor.

More details about the synthesis and characterization procedures can be found in the previous chapter.

5.2.3. Pyridine/Piperidine/Pentylamine Reactivity

The reactivities of the three amines (pyridine, piperidine and *n*-pentylamine) were determined separately in a trickle-bed reactor, employing liquid phase conditions at 3.1 MPa and various temperatures. The apparatus and procedure for the reactivity tests are described in detail in the previous chapter.

Before each change in conditions and reagent, the reaction system was allowed to run for 60 h to be sure it had reached a steady-state condition. Liquid samples were collected at regular intervals, and the average of the steady-state values was used for the calculation of conversion and product distribution. Periodic recheck of catalytic activity at standard conditions after several experiments demonstrated that there was no deactivation. Again, as with the amines work, measurements were carried out for several months on each catalyst. The liquid samples were analyzed off-line by gas chromatography (Hewlett-Packard, 5890 Series II) using a fused silica capillary column (CPSIL-5CB) and a flame ionization detector. The reaction products were identified by GC-MS (VG Quattro, triple quadrupole, EI positive method) and the results of the identification were confirmed by the injection of standard compounds. The retention times and response factors for all reagents and products are shown in Table 4.2. Analysis of the gas phase revealed the presence of the same light hydrocarbons found in the liquid phase. Since only the analysis of the liquid phase was performed during the tests, vapor-liquid equilibrium curves [14] were used to obtain a correction factor for each of the C_5

hydrocarbons in order to take into account the products remaining in the gas phase. The mass balance was close to 100% (± 10%).

5.3. Results

Conversions of pyridine, piperidine, and *n*-pentylamine were investigated as a function of temperature for the carbide catalysts ($NbMo_2C$, Mo_2C, and NbC) and the sulfide reference MoS_2/SiO_2 (Figure 5.1). All the values of conversion plotted in Figure 5.1 have an error in the range of ± 5% (high conversions) to ± 15% (low conversions).

The results obtained for the monometallic NbC catalyst are not presented here and will not be discussed any further, since they indicated the same conversion levels obtained for a blank reactor. SiO_2 was used as a support for the sulfide catalyst due to its inert character and consequently small interaction with the sulfided phase [15]. The same conversion trend was found for all the catalysts (Figure5.1). The reactivity of *n*-pentylamine was relatively high, while the conversion of piperidine was low, especially at low temperatures. As will be discussed later, the hydrogenation route of pyridine to piperidine is not limited by thermodynamic equilibrium at the experimental conditions employed in this study. Details about the characterization results for the catalysts used during this work can be found in previous chapter.

a)

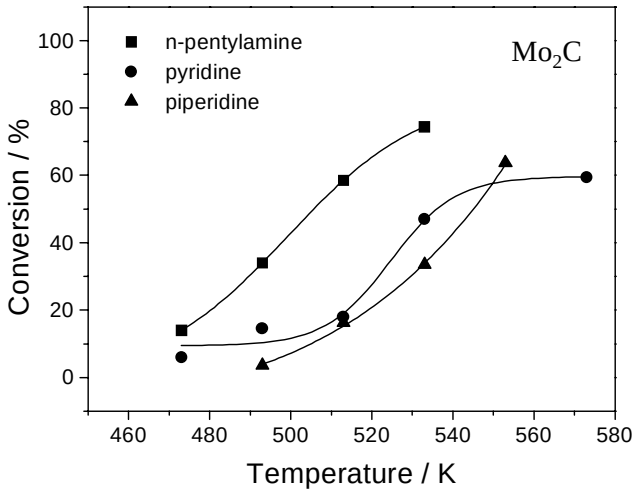

b)

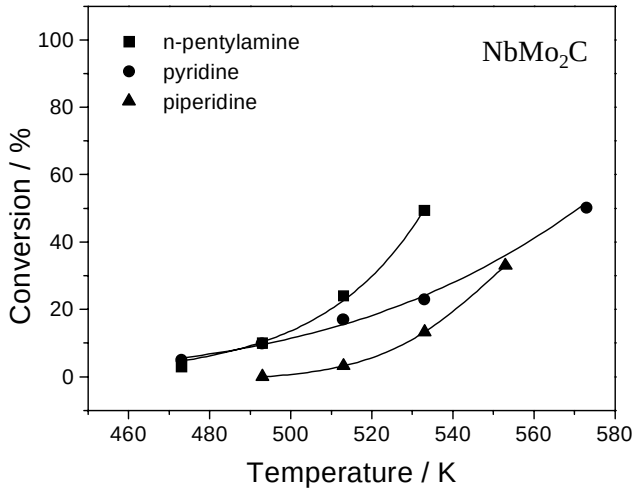

c)

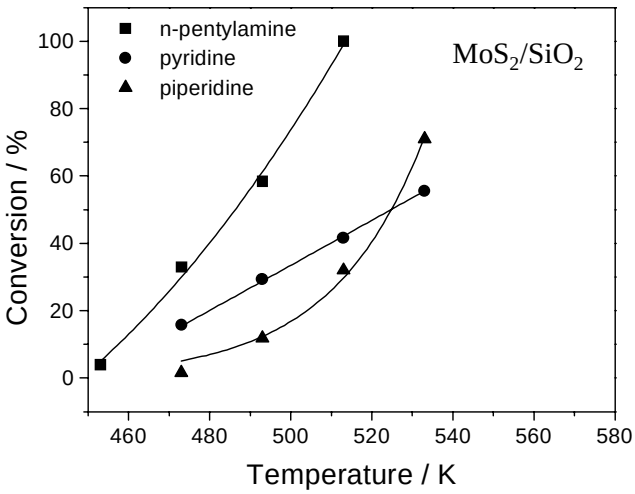

Figure 5.1. Conversion of *n*-pentylamine, piperidine, and pyridine over: a) Mo_2C; b) $NbMo_2C$; c) MoS_2/SiO_2.

The effect of temperature on the product distributions of *n*-pentylamine, piperidine and pyridine for Mo_2C, $NbMo_2C$, and MoS_2/SiO_2, is shown respectively in Figures 5.2, 5.3, and 5.4. Figure 5.2 presents the results for the *n*-pentylamine reaction. The left panels show the conversion and the overall product selectivity for C_5 hydrocarbons, condensation products, and sulfur products. The right panels show the details of the C_5 hydrocarbon distribution. Pentane was found in the largest amounts, followed by 1-pentene, *trans*-2-pentene, and *cis*-2-pentene at higher conversions. In the case of $NbMo_2C$, the only C5 product was pentane, and a right panel is not shown (Figure 5.2b). As discussed in the previous chapter, these products are the result of a β-elimination type of mechanism. The condensation products were the N-containing compounds, dipentylamine and tripentylamine, which come from a disproportionation reaction. Tripentylamine was only present in small amounts at higher temperatures over the carbide catalysts. The condensation products are easily formed and are the main products in the low temperature range. They are also reported to be more reactive for C-N bond cleavage than is the primary amine [3]. In the case of *n*-pentylamine, the sulfur product was pentanethiol, formed by a substitution mechanism between the pentylamine (substrate) and hydrogen sulfide (nucleophile). Due to its high reactivity toward C-S bond cleavage, only small amounts of pentanethiol were found among the products. In comparing the three catalysts, it can be seen that Mo_2C (Figure 5.2a) and MoS_2/SiO_2 (Figure 5.2c) have the highest activities, and $NbMo_2C$ (Figure 5.2b) has the lowest.

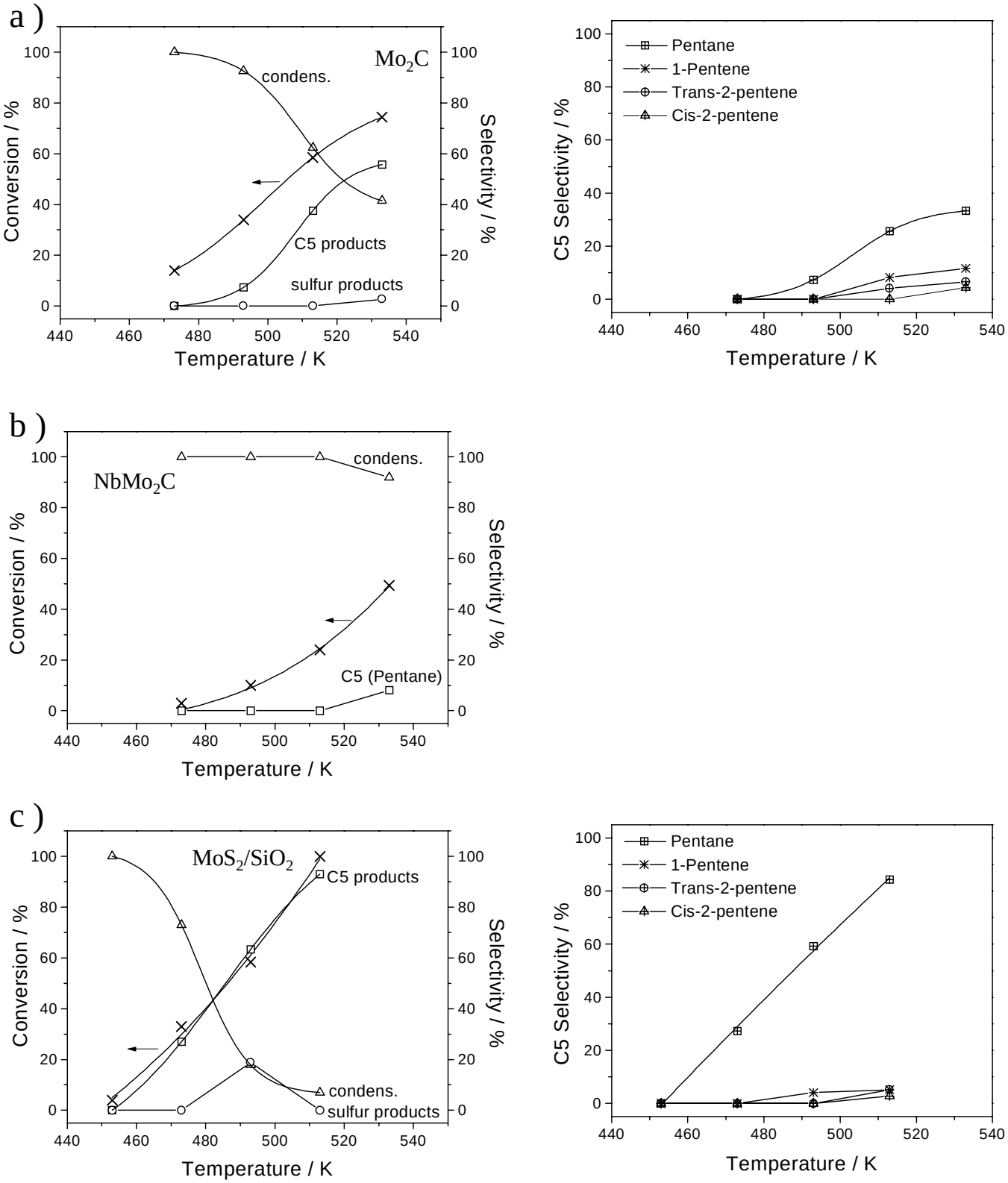

Figure 5.2. Conversion and product distribution for the *n*-pentylamine reaction over: a) Mo_2C; b) $NbMo_2C$; c) MoS_2/SiO_2.

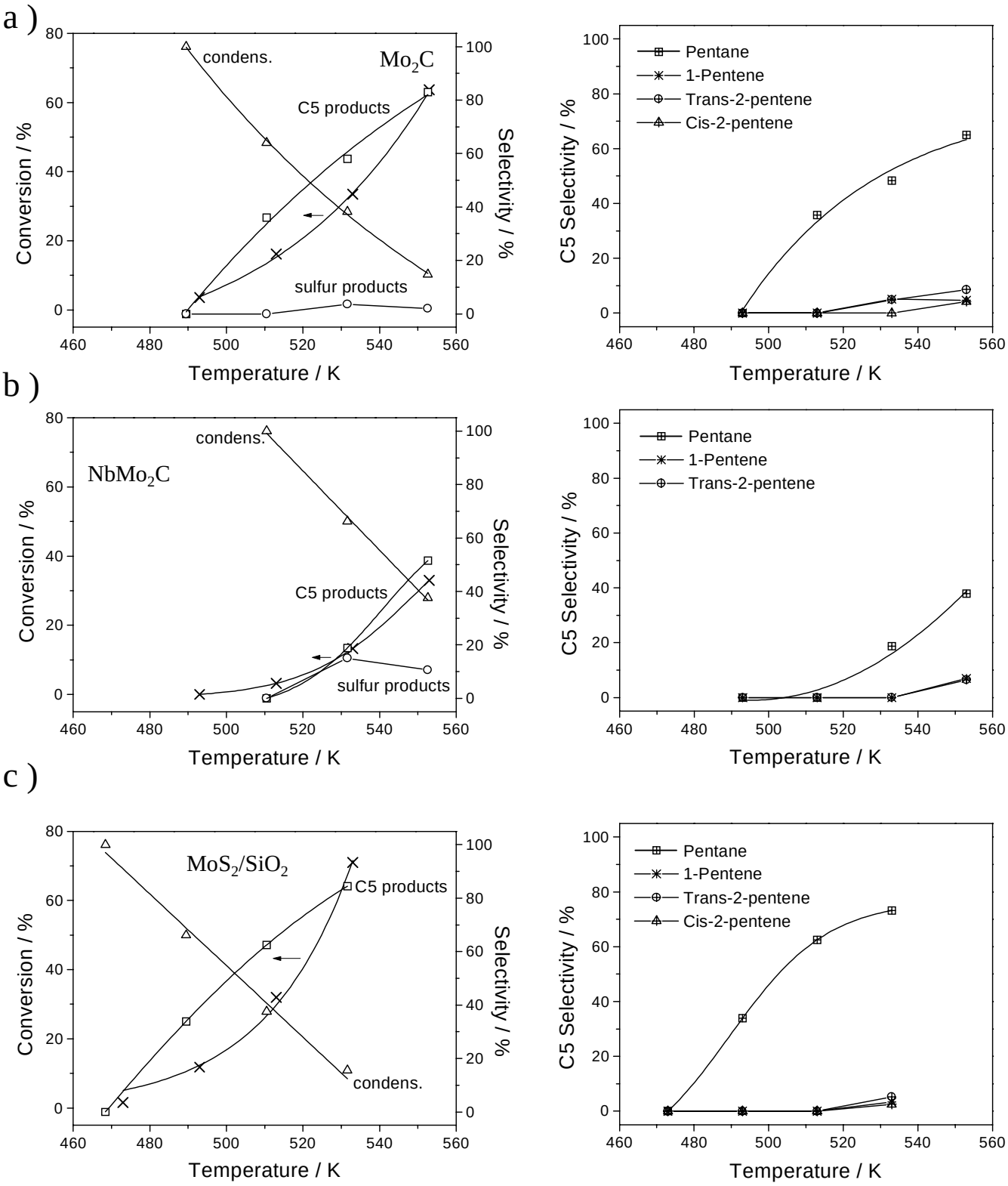

Figure 5.3. Conversion and product distribution for the piperidine reaction over: a) Mo_2C; b) $NbMo_2C$; c) MoS_2/SiO_2.

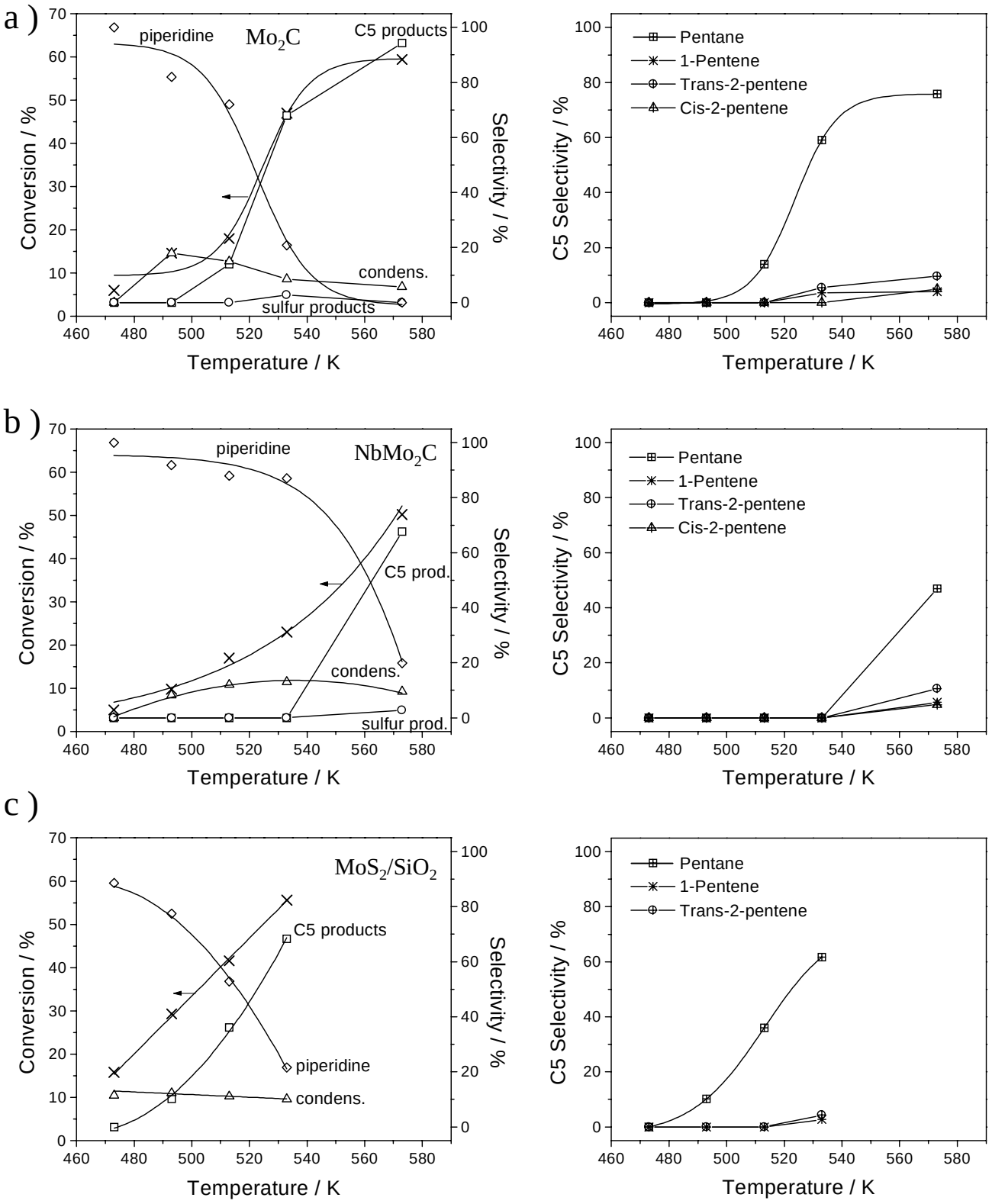

Figure 5.4. Conversion and product distribution for the pyridine reaction over: a) Mo_2C; b) $NbMo_2C$; c) MoS_2/SiO_2.

Figure 5.3 shows the results for piperidine. Again, the left panels show the conversion and overall selectivity, while the right panels show the C5 product distribution. Pentylamine was never found among the products, while substantial amounts of condensation compounds were observed at low temperatures. In the case of the piperidine reaction, the condensation products were N-pentylpiperidine and in very low concentrations, N-butylpiperidine. The absence of *n*-pentylamine indicates that, at low temperatures, the most important consecutive reaction is not the formation of pentylamine by the opening of the piperidine ring, but the metathesis of a piperidine molecule and *n*-pentylamine into ammonia and N-pentylpiperidine (Scheme 5.2). The sulfur products identified during this reaction were: tetrahydro-2H-thiopyran and small amounts of tetrahydro-2-methyl-thiophene. A reaction pathway is suggested for the formation of these molecules in the presence of hydrogen sulfide (Scheme 5.3) [16]. In this scheme, the piperidine ring is opened as a result of C-N bond scission. Part of this compound undergoes a nucleophilic substitution reaction with hydrogen sulfide to give 4-pentene-1-thiol. The latter then cyclizes to tetrahydro-2H-thiopyran and tetrahydro-2-methyl-thiophene. The C_5 hydrocarbons found were the same as the ones found in the HDN of *n*-pentylamine with a similar product distribution. No pyridine was found among the products since the dehydrogenation reaction of piperidine is not thermodynamically favored at the reaction conditions used during this study. Among the C5 hydrocarbon products, for all catalysts, the main product was pentane, while smaller amounts of pentenes were obtained at higher conversions.

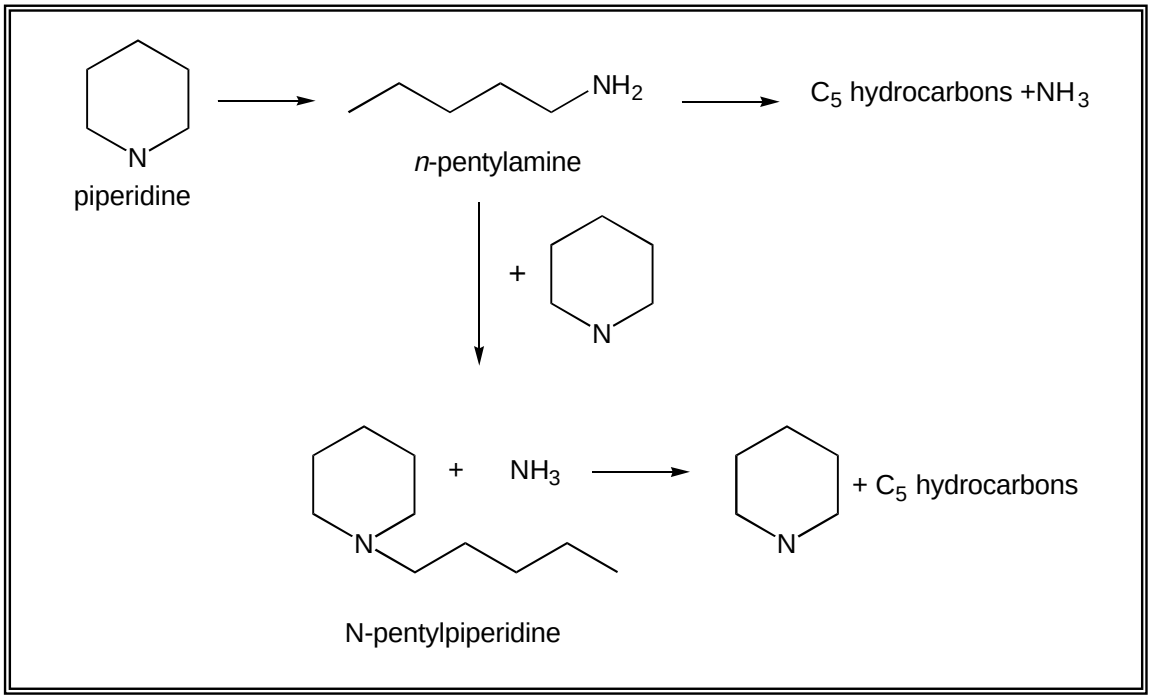

Scheme 5.2. Reaction scheme for HDN of piperidine.

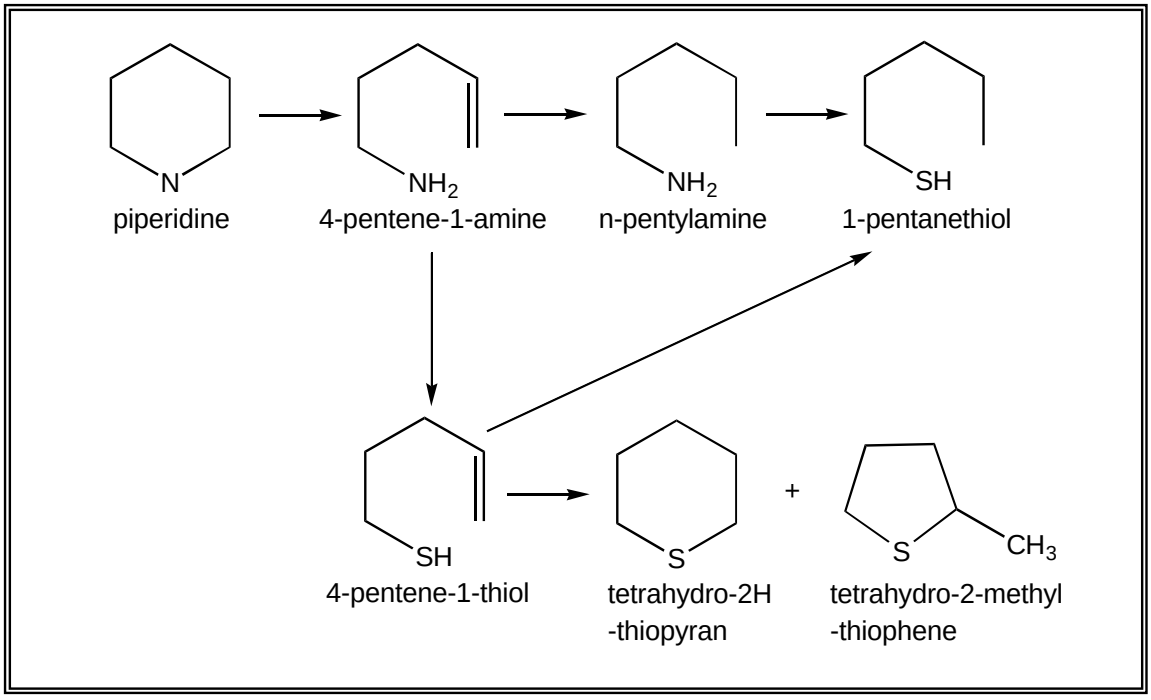

Scheme 5.3. Reaction pathway for formation of sulfur products.

Figure 5.4 shows the results for the pyridine reaction. Once again, the left panels report conversion and overall selectivity, while the right panels show the C5 product distribution. The overall distribution is in agreement with that obtained in the piperidine reaction. At low conversions the major product was piperidine, arising from the first hydrogenation step, and a small amount of N-pentylpiperidine. As conversion increased, C_5 hydrocarbons began to be produced, and pentane remained the major product.

Analysis of the product distribution for piperidine and pyridine over the three catalysts at the same conversion levels are presented in Figures 5.5 and 5.6. *n*-Pentylamine is not analyzed further since the deamination of the primary amine was fast (Figure 5.1) compared to the denitrogenation of the heterocyclic nitrogen compounds. MoS_2/SiO_2 showed a slightly higher amount of denitrogenated products compared to the carbide catalysts for the piperidine reaction (Figure 5.5). However, the carbides presented a considerable superiority regarding the concentration of HDN products when pyridine was used as reagent (Figure 5.6).

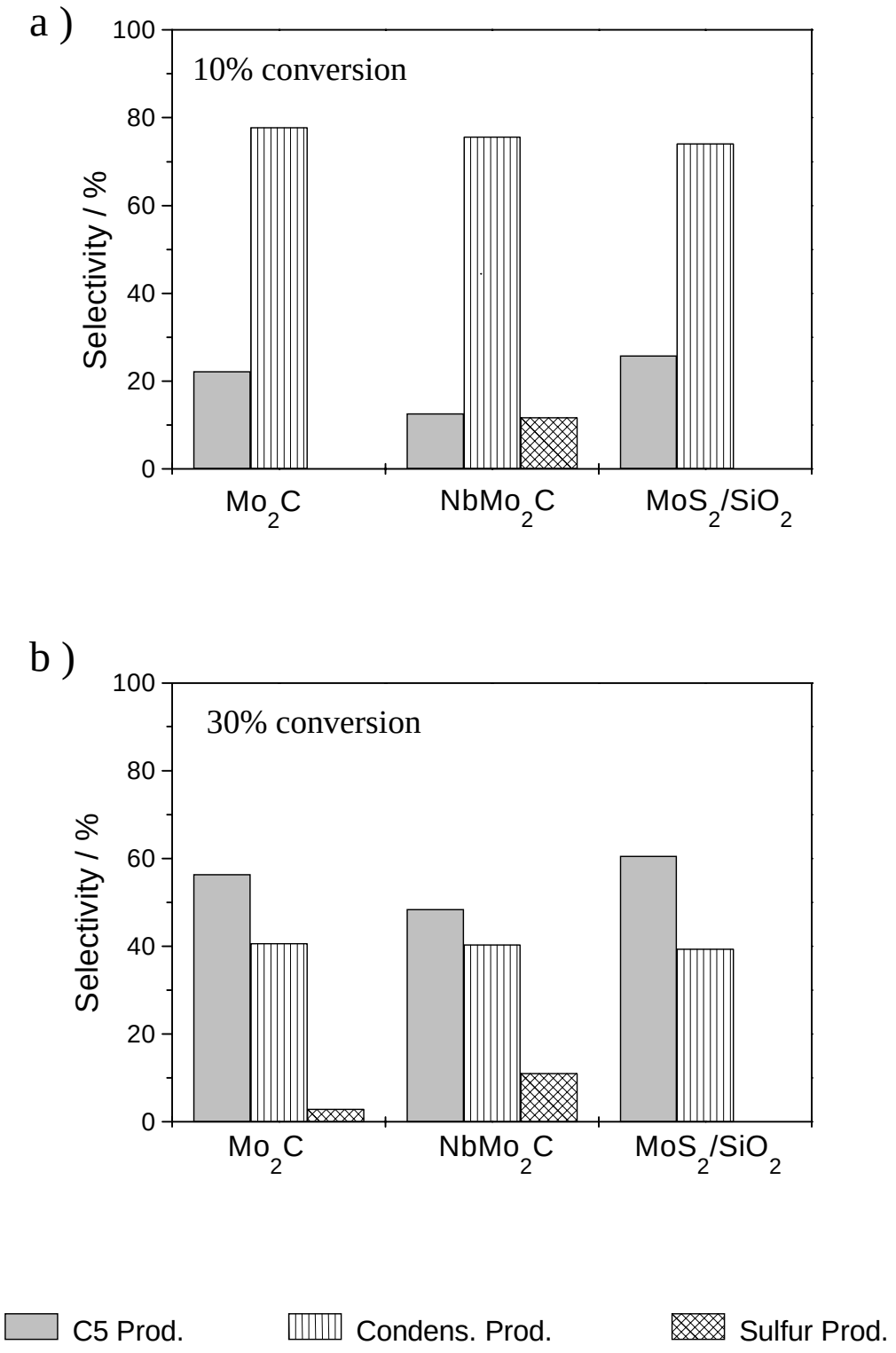

Figure 5.5. Piperidine product distribution at constant conversion levels: a) 10% conversion; b) 30% conversion.

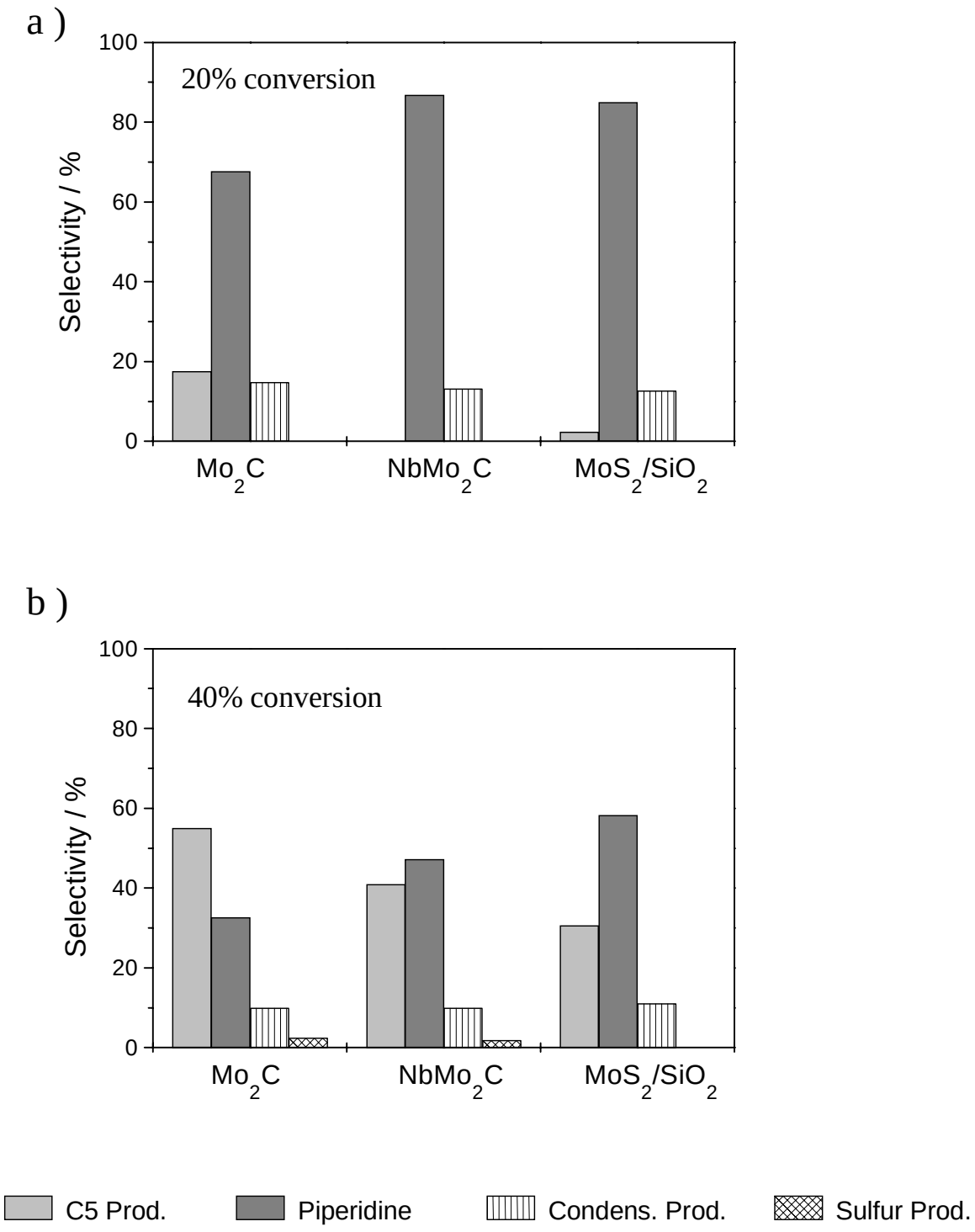

Figure 5.6. Pyridine product distribution at constant conversion levels: a) 20% conversion; b) 40% conversion.

5.4. Discussion

Comparing the values of conversion of *n*-pentylamine (Figure 5.1) with the two heterocyclic molecules, piperidine and pyridine, it is clear from the low temperature of reaction that the aliphatic amine has a very high reactivity, regardless of the catalyst used. Further evidence of its high reactivity is finding that *n*-pentylamine is never formed as an intermediate product for the reactions of piperidine (Figure 5.3) and pyridine (Figure 5.4). Therefore, the rate-determining step in the denitrogenation of pyridine is either hydrogenation or ring-opening. The nature of the rate-determining step may vary according to the experimental conditions. In the reaction network for the HDN of pyridine (Scheme 5.1) we will consider only the first two steps to be kinetically significant.

In this simplified reaction network, we have purposely avoided the use of the double arrow between pyridine and piperidine, which indicates reversible reaction. The thermodynamic equilibrium equation [17] below indicates that at our experimental conditions , P_{H2} = 450 psi (30.6 atm) and 450 K < T < 570 K, the equilibrium lies well to the right:

$$\ln K = {}^{23470}\!/_{T} - 46.06 + 3\ln\left({}^{P_{H_2}}\!/_{P^0}\right) \qquad (1)$$

where K = [piperidine]/[pyridine], [T] = K, and P^o = 1 atm. Values of K are 1.27×10^7 at 450 K and 2.17×10^2 at 570 K. Additionally, the fact that no pyridine was found as product when piperidine was used as reagent (Figure 5.3) confirms that the pyridine-piperidine equilibrium is completely on the piperidine side.

The same products were identified during the pyridine and piperidine reactions for all catalysts (Figures 5.3 and 5.4). The main difference lies in the much smaller amount of condensation products found when pyridine was the reagent. Also in the case of the pyridine reaction, it was found that hydrocarbons were formed at higher temperatures as piperidine disappeared from the products, indicating that ring opening preceded hydrocarbon formation.

Although the sulfide catalyst presented consistently higher conversions than the carbides at the same temperature, the latter had a superior selectivity towards HDN products at the same conversion levels (Figure 5.6). The superiority is more evident at higher conversions. For example, at conversions of 40%, piperidine is still the major product over the sulfide catalyst, while Mo_2C already shows high yields of hydrocarbons. These results indicate that the ratio of rate constants ($r = k_2/k_1$) of the second step (hydrogenolysis of piperidine) to the first step (hydrogenation of pyridine) is smaller for the sulfide catalyst compared to the carbides. In order to obtain a better understanding of this situation, the relative rates are quantified below. Taking the simplified reaction network illustrated in Scheme 5.1, it is assumed that both steps are first-order and irreversible. This is reasonable considering that most studies [3,10,12] of the pyridine/piperidine reaction on sulfide catalysts can be fit to a first-order kinetic model and that the hydrogenation of pyridine is practically irreversible at our given reaction conditions. In this case, the rate of consumption of pyridine and the rate of formation of the intermediate, piperidine, would be represented as follow:

$$-\upsilon_{PYR} = k_1[PYR] \qquad (2)$$

$$\upsilon_{PIP} = k_1[PYR] - k_2[PIP] \quad (3)$$

Since $-\upsilon_{PYR}$ represents the rate of formation of all products, the selectivity (S) for the piperidine intermediate can be defined as:

$$S = \frac{\upsilon_{PIP}}{-\upsilon_{PYR}} = 1 - \frac{k_2[PIP]}{k_1[PYR]} \quad (4)$$

The ratio, r, between the two rate constants, k_2 and k_1, is obtained by rearranging the above expression:

$$r = \frac{k_2}{k_1} = (1 - S)\left(\frac{PYR}{PIP}\right) \quad (5)$$

Values of selectivity and conversion were obtained for each catalyst for various temperatures in the range used during the study of the pyridine reaction (Figure 5.4) and are summarized in Table 5.1. In order to obtain more points at lower temperatures and to smooth the fits, data were extrapolated from Figure 5.4. The ratio of [PYR]/[PIP] is calculated from the values of conversion (X) and selectivity, since $S = \frac{[PIP]}{[PYR]_0 - [PYR]}$ and $X = \frac{[PYR]_0 - [PYR]}{[PYR]_0}$, which gives:

$$\frac{[PYR]}{[PIP]} = \frac{(1 - X)}{SX} \quad (6)$$

Table 5.1. Pyridine HDN results for Mo_2C, $NbMo_2C$, and MoS_2/SiO_2. (X = conversion of pyridine and S = selectivity of piperidine)*

	T / K	X / %	S / %	[PYR]/[PIP]	$r = k_2/k_1$
Mo_2C	489	10.0	91.5	9.84	0.836
	504	12.8	83.6	8.20	1.345
	514	20.0	66.0	6.10	2.073
	518	25.0	57.6	5.20	2.206
	522	30.0	47.7	4.90	2.562
	528	40.0	32.8	4.60	3.091
	532	45.0	24.0	5.10	3.875
	536	50.0	16.4	6.10	5.098
$NbMo_2C$	506	13.2	93.2	7.06	0.480
	533	23.0	84.8	3.95	0.601
	542	27.3	78.7	3.38	0.720
	550	32.5	69.5	2.99	0.912
	558	38.2	57.1	2.83	1.214
	563	42.4	47.2	2.88	1.521
	569	47.8	33.1	3.30	2.208
MoS_2/SiO_2	480	20.0	85.0	4.71	0.707
	487	25.0	80.0	3.75	0.750
	495	30.0	74.7	3.13	0.792
	503	35.0	66.6	2.79	0.932
	510	40.0	58.0	2.59	1.088
	517	45.0	48.7	2.51	1.287
	525	50.0	36.4	2.75	1.750

*Values were interpolated from smoothed out conversion and selectivity curves in Figures 5.2-5.4

Table 5.1 also shows the calculated values for r obtained for each catalyst. It can be observed that the ratio, r, for the Mo_2C catalyst, which presents better selectivity for hydrocarbons products, is consistently higher than the values obtained for the sulfide catalyst, as expected. In all cases, the ratio increases with temperature.

The difference in activation energies between the two steps of reaction can be related to the ratio, r, through the Arrhenius equation, as shown below:

$$r = \frac{A_2}{A_1} \exp\left[- \left(E_2 - E_1 \right) \Big/ RT \right] \qquad (7)$$

Here A_1 and A_2 are the preexponential factors.

A plot of ln(r) vs. 1/T is given for all the catalysts (Figure 5.7) and the difference in activation energies between the first two steps of the pyridine HDN reaction is obtained from the slope of the plots. The points at high temperatures were not considered for the linear fit. In the case of the sulfide catalyst, the rupture of the heterocyclic ring requires 33.2 kJ mol^{-1} more than the hydrogenation of pyridine, while in the other extreme, for Mo_2C, the difference rises to 75.3 kJ mol^{-1}. The larger difference in activation energy combined with higher ratio of preexponential factor (A_2/A_1) is responsible for higher selectivities for hydrocarbon products at high temperatures and conversion. The bimetallic presented an intermediate value for the difference of activation energies between the second and first step equal to 46.1 kJ mol^{-1}. Selectivity for HDN products was also intermediate at higher temperatures as can be observed in Figure 5.6.

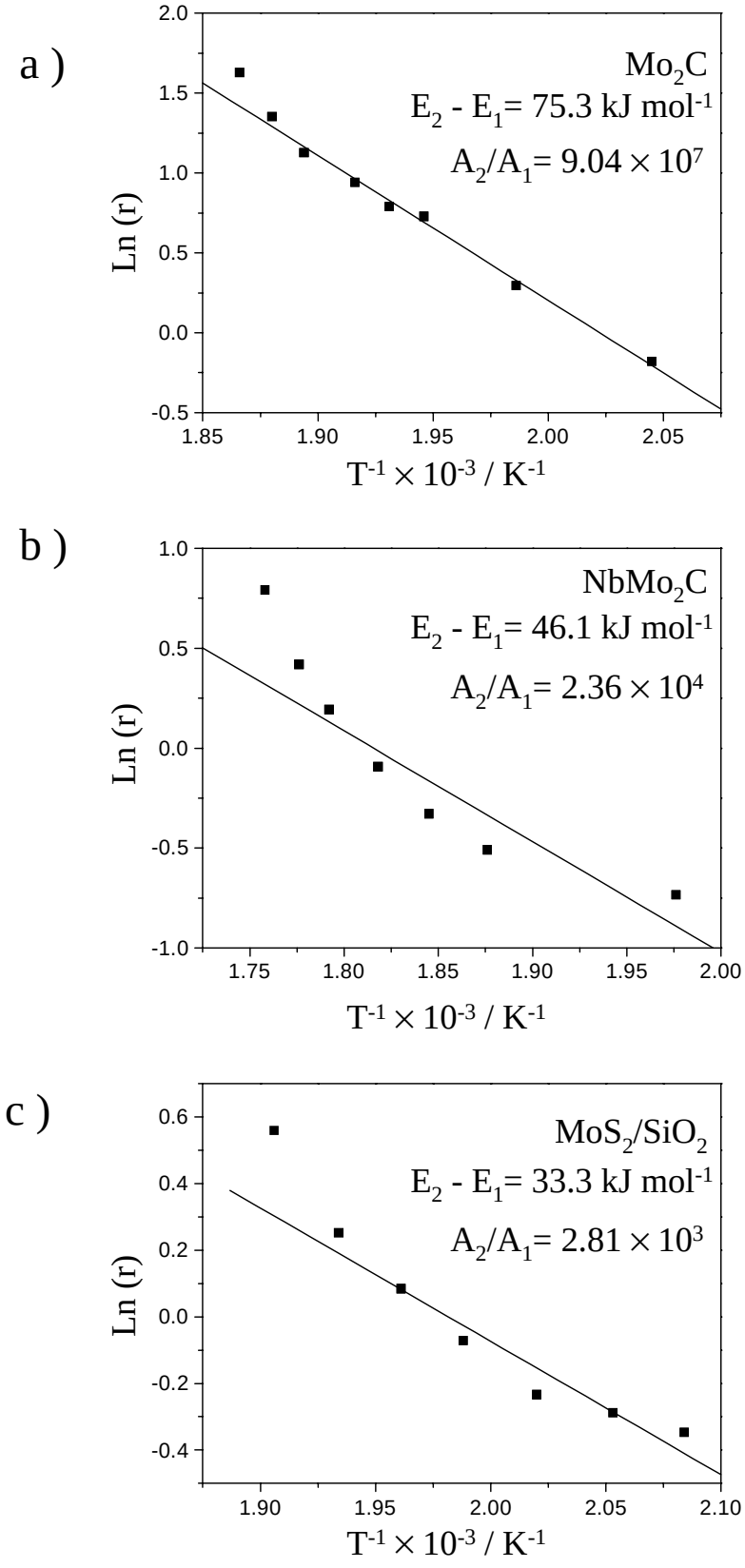

Figure 5.7. Ln (r) vs 1/T plots for: a) Mo_2C; b) $NbMo_2C$; c) MoS_2/SiO_2.

Although instructive, this simplified analysis is not a rigorous representation of the actual catalytic reaction mechanism for pyridine HDN. A more detailed mechanism should describe the adsorption of the reagents on the catalyst surface and the surface reaction. Again, only the slow and equilibrated steps were taken into account during the development of the following and more detailed reaction scheme (Scheme 5.4). The scheme does not show the adsorption of hydrogen. The literature [7,8,9] indicates that hydrogen and the nitrogen-bases are adsorbed on different catalytic sites and at the high H_2 partial pressures used in these studies the hydrogen sites are likely to be saturated. The network shown involves the so-called rake mechanism (Scheme 5.4) [18]:

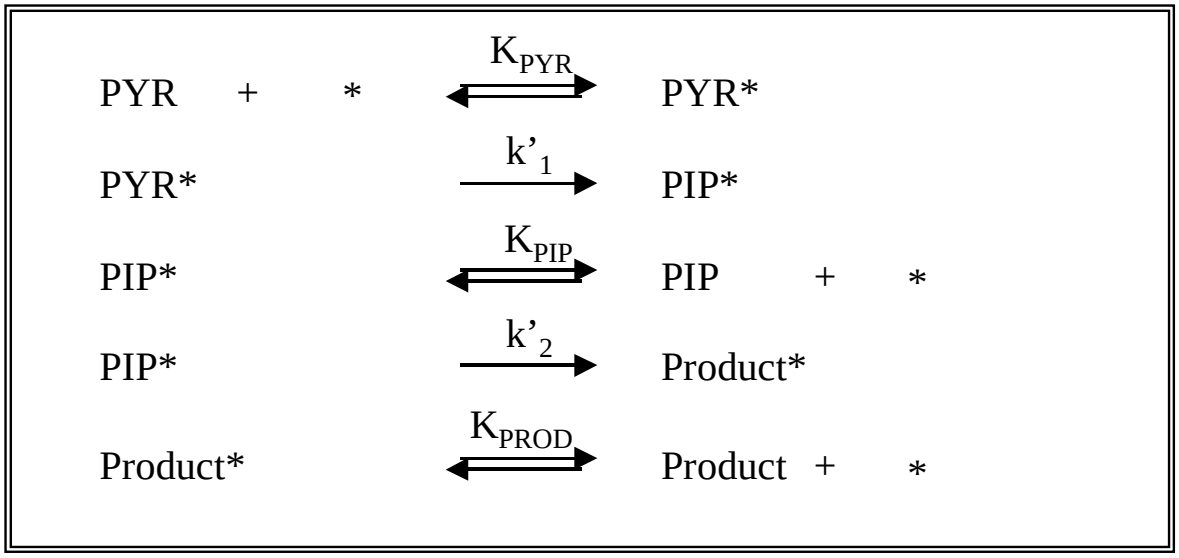

Scheme 5.4. Rake mechanism for the reaction network.

According to Scheme 5.4, at steady-state, the rates of the two unequilibrated steps, (υ'_1 and υ'_2) should be equal:

$$\upsilon'_1 = k'_1[\text{PYR}*] \tag{8}$$

$$\upsilon'_2 = k'_2[\text{PIP}*] \tag{9}$$

From these equations, (8) and (9), and the equilibrium expressions for [PYR*] and [PIP*], we obtain a relation involving the hydrogenation of pyridine and the piperidine ring-opening steps:

$$\frac{k'_2}{k'_1} = \frac{K'_{\text{PYR}}[\text{PYR}]}{K'_{\text{PIP}}[\text{PIP}]} \tag{10}$$

In this analysis, the ratio of rate constants, k'_2/k'_1, involves contributions from the equilibrium constants of adsorption of pyridine and piperidine. We are unable to get these constants from the limited data available, but it can be seen that the value of k'_2/k'_1 is different from that of r, obtained by the simple analysis. Rearranging equation 10, we define a new r':

$$r' = \frac{k'_2 K'_{\text{PIP}}}{k'_1 K'_{\text{PYR}}} = \frac{[\text{PYR}]}{[\text{PIP}]} \tag{11}$$

For each temperature and conversion, a new value for the ratio, r', between the rate of the ring-opening and hydrogenation step was obtained based on the ratio of concentrations of pyridine and piperidine, which are given on Table 5.1. The values of r' for the Mo_2C catalyst, which presents better selectivity for hydrocarbons products, is consistently higher than the values obtained for the sulfide catalyst. From equation 11, a new Arrhenius expression (equation 12) is derived:

$$r' = \frac{A'_2 A_{PIP}}{A'_1 A_{PYR}} \exp\left[- \frac{\left[\left(E'_2 - \Delta H'_{PIP} \right) - \left(E'_1 - \Delta H'_{PYR} \right) \right]}{RT} \right] \qquad (12)$$

For each of the three catalysts, a plot of ln(r') vs. 1/T was produced (Figure 5.8). The linear regression was again obtained after excluding the high temperature points. Based on the Arrhenius expression (equation 12), the slope of the plots is related to the activation energies and the change in enthalpies for the adsorption steps. The overall energy changes are defined on the energy diagrams sketched on Figure 5.9. In this case, the Arrhenius plots produced a positive slope for the low temperature points, consequently the difference $\left(E'_2 - \Delta H'_{PIP} \right) - \left(E'_1 - \Delta H'_{PYR} \right)$, which includes the heats of adsorption of pyridine and piperidine, gives a negative value. For the sulfide, the difference is equal to – 40.0 kJ mol^{-1}, while for Mo_2C is – 45.6 kJ mol^{-1}. The bimetallic presented again an intermediate value equal to – 42.6 kJ mol^{-1}. The similarity in the values for all catalysts can be rationalized if there is a linear free energy relationship between E' and $\Delta H'$ for the adsorption of pyridine and piperidine, and if the difference in the heats of adsorption are similar. This similarity was an unexpected and an *a priori*

unlikely result, but it suggests that the mechanism on the three catalysts are likewise similar.

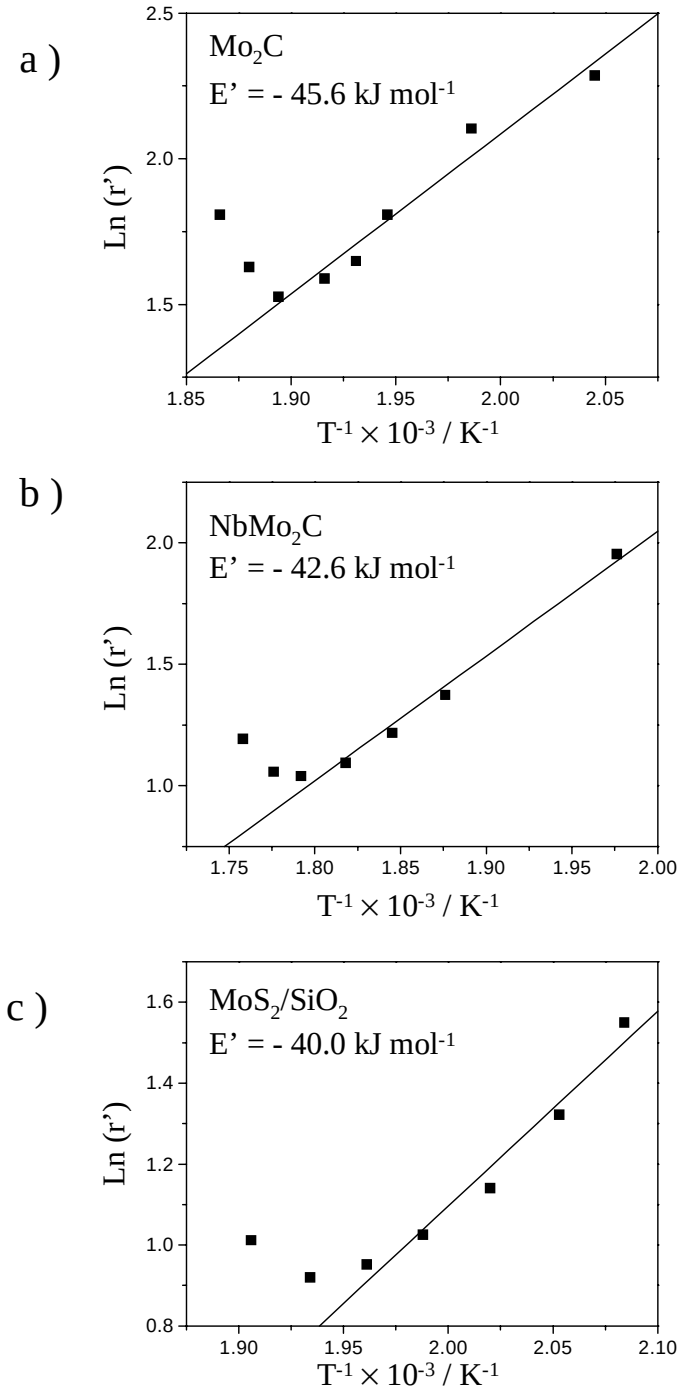

$$E' = \left(E'_2 - \Delta H'_{PIP}\right) - \left(E'_1 - \Delta H'_{PYR}\right)$$

Figure 5.8. Ln (r') vs 1/T plots for: a) Mo_2C; b) $NbMo_2C$; c) MoS_2/SiO_2.

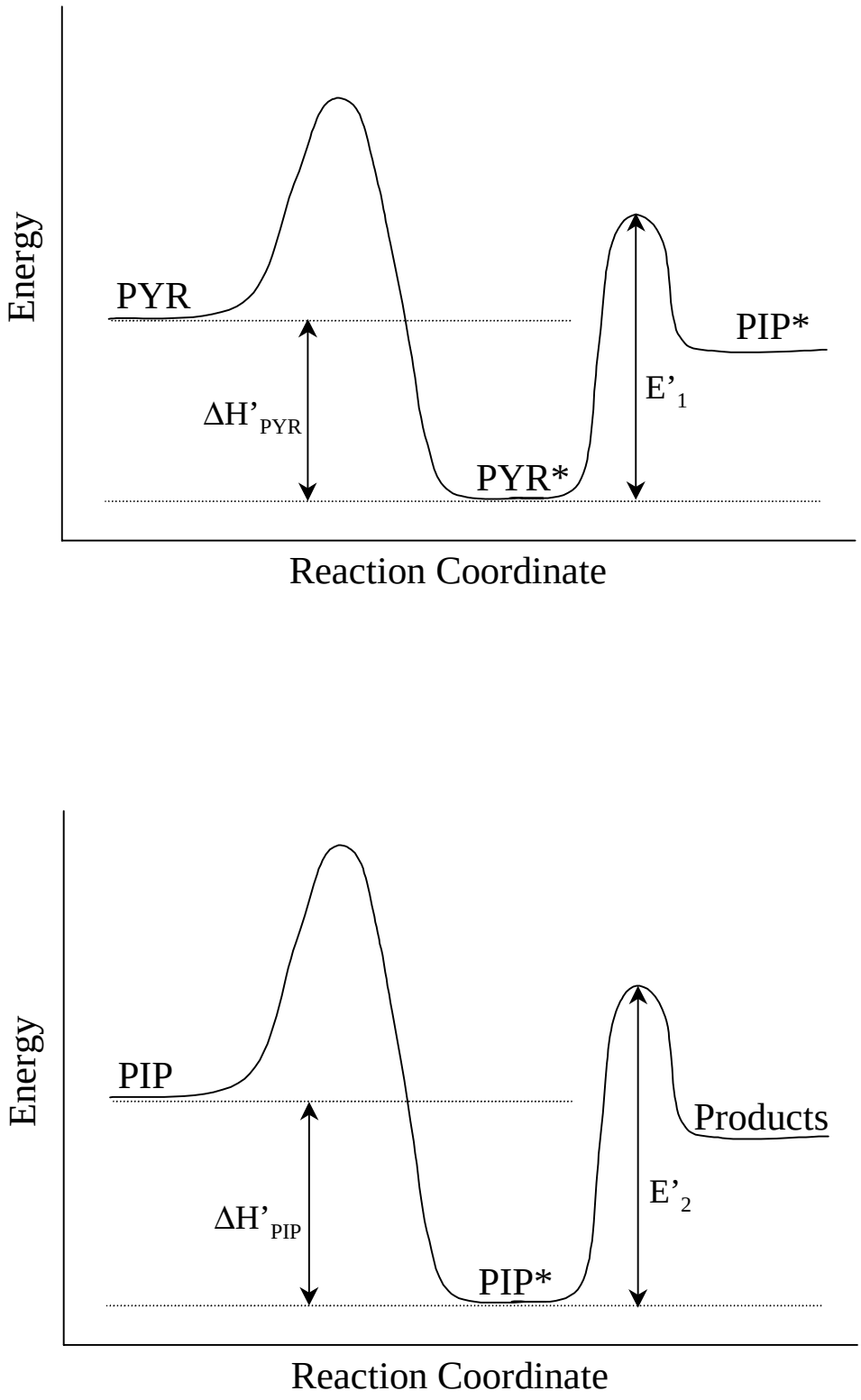

Figure 5.9. Energy diagram sketch.

An overall comparison between the carbide catalysts and the sulfide reference presents a very interesting aspect. The sulfide catalyst showed higher activity than the bimetallic carbide for all the probe molecules tested on this study, which were: *n*-pentylamine, piperidine and pyridine (Figure 5.1). This is true whether the CO and O_2 uptakes or the number of Brønsted-acid sites were used for calculation of turnover rates. On the other hand, the situation is completely reversed when the catalysts were compared for the simultaneous HDN of quinoline and HDS of dibenzothiophene. As described in the previous chapter, for this catalytic test, MoS_2/SiO_2 presented small HDN (10 %) and HDS (26 %) conversions, compared to the results for $NbMo_2C$, which had high HDN (57%) and HDS (59%) conversions. Those results suggest that comparison of HDN activities have to be strictly related to the nature and structure of the probe molecules. For example, some studies in the literature [19,20] analyze the effect of alkyl substituents on the HDN of pyridine. The compounds derived from pyridine presented a large range of activity change [19]. In fact, the presence of substituents slows down both hydrogenation and hydrogenolysis [20]. If quinoline is viewed as a benzo-substituted pyridine, the attachment of a benzene ring should have an even stronger influence than the alkyl substituents on the reactivity of pyridine. Another important aspect that differentiates the two molecules, pyridine and quinoline, is that the rate-limiting step of quinoline HDN is supposed to be the hydrogenation of the benzenic ring [6]. This fact makes difficult any comparison with the HDN of pyridine, which does not involve such a reaction.

The nature of the active sites is another point that should be addressed in this discussion. Studies [9,21,22] using sulfide catalysts for the HDN reaction associate two

types of catalytic sites to the two different functions, hydrogenation and C-N bond cleavage. The sites for hydrogenation are thought to be related to sulphur anion vacancies while the sites active for the cleavage of the C-N bond seem to be acidic. In the previous chapter we have identified nucleophilic sulfide and Brønsted-acidic sites as required for C-N bond cleavage on both carbides and sulfide. Therefore, different cases should be considered depending on the distance between the acidic and the hydrogenation sites. When they are adjacent, they form an entity able to catalyze the hydrogenation reactions as well as the C-N bond cleavage. The difference of the structure between the two molecules, pyridine and quinoline, together with the surface distribution of active sites on a given catalyst, might explain the large range of activities found for these two molecules with the same catalyst.

5.5. Conclusions

In this study, we investigated the pyridine HDN and the role of the intermediates, piperidine and *n*-pentylamine, over $NbMo_2C$, Mo_2C, NbC and MoS_2/SiO_2. The reactions were carried out in liquid phase and the N-containing molecules were studied separately. The products identified from the pyridine, piperidine and *n*-pentylamine reactions were the same for the carbides, as well as the sulfide catalyst, indicating that the reaction pathway was the same on all catalysts. Among the hydrocarbons products, 1-pentene was the most abundant olefin providing evidence for the contribution of a β-elimination type of mechanism. Comparison of the activities of the three molecules showed the same trend for all the catalysts. The *n*-pentylamine reaction is very fast when compared to the

hydrogenation of pyridine and the C-N bond cleavage of piperidine, as shown by the absence of *n*-pentylamine among the products of reaction.

The carbide catalysts showed higher selectivity towards HDN products than the sulfide catalyst at the same conversion levels. A first-order kinetic model gave a simple explanation for the results. The higher selectivity was related to the ratio between the rate constants of the two consecutive reactions: hydrogenation of pyridine and ring opening of piperidine. The higher the ratio, the higher the selectivity for hydrocarbons at high temperatures and conversions. Although the bimetallic carbide presented better selectivity at high conversions than the sulfide, the latter was more active when comparison was based on the same temperatures. The higher activity of the sulfide for the pyridine HDN compared to the small quinoline HDN activity allows us to conclude that the HDN reaction mechanism depends greatly on the structure of the N-containing molecule and the surface site distribution.

References

[1] H. Topsøe, B.S. Clausen, F.E. Massoth, Hydrotreating Catalysts, Science and Technology, Springer, New York, 1991, p.133.

[2] T.C. Ho, Catal. Rev.-Sci. Eng. 301:1 (1988) 117.

[3] H. Shulz, M. Schon, N.M. Rahman in L. Cerveny (Ed.), Studies in Surface Science and Catalysis, Elsevier, Amsterdam, 1986, Vol. 127, Chap. 6.

[4] C.N. Satterfield, J.F. Cochetto, Ind. Eng. Chem. Proc. Des. Dev. 20 (1981) 53.

[5] M. Cattenot, J.-L. Portefaix, J. Afonso, M. Breysse, M. Lacroix, G. Perot, J. Catal. 173 (1998) 366.

[6] G. Perot, Catal. Today 10 (1991) 447.

[7] J.K. Minderhoud, J.A.R. Van Veen, Fuel Proc. Tech. 35 (1993) 87.

[8] R.T. Hanlon, Energy Fuels 1 (1987) 424.

[9] S.H. Yang, C.N. Satterfield, J. Catal. 81 (1983) 168.

[10] H.G. McIlvried, Ind. Eng. Chem. Proc. Des. Dev. 10:1 (1971) 125.

[11] J. Sonnemans, P. Mars, J. Catal. 31 (1973) 209.

[12] C.D. Ajaka, R.S. Mann, Ind. J. of Tech. 31 (1993) 131.

[13] A. Calafat, J. Laine, A. Lopez-Agudo, Catal. Lett. 40 (1996) 229.

[14] S.T. Hadden, H.G. Grayson, Hydroc. Proc. Petrol. Refin. 40 (1961) 207.

[15] M. Breysse, J.L. Portefaix, and M. Vrinat, Catal. Today 10 (1991) 489.

[16] M. Cerny, Coll. Czech. Chem. Comm. 47 (1982) 928.

[17] W.V. Steele, R.D. Chirico, Topical Report for the U.S. Department of Energy, IIT Research Institute, Barstlesville, Oklahoma, 1992.

[18] M. Boudart, G. Djéga-Mariadassou, Kinetics of Heterogeneous Catalytic Reactions, 1st Ed., Princeton University Press, New jersey, 1984.

[19] K.E. Cox, L. Berg, Chem. Eng. Prog. 56 (1962) 54.

[20] M. Cerny, Coll. Czech. Chem. Comm. 44 (1979) 85.

[21] S.H. Yang, C.N. Satterfield, Ind. Eng. Chem. Proc. Des. Dev. 23 (1984) 20.

[22] M.Callant, K.A. Holder, P. Grange, B. Delmon, Bull. Soc. Chim. Belg. 104:4 (1995) 245.